Search for ^{21}B

A. Ozawa,[1] Y. Yamaguchi,[1,2] M. Chiba,[1,3] R. Kanungo,[1] K. Kimura,[4] S. Momota,[5] T. Suda,[1] T. Suzuki,[2] I. Tanihata,[1] T. Zheng,[1,6,7] S. Watanabe,[2] T. Yamaguchi,[1,8] and K. Yoshida[1]

[1]*The Institute of Physical and Chemical Research (RIKEN), Hirosawa 2-1, Wako-shi, Saitama 351-0198, Japan*

[2]*Department of Physics, Niigata University, Niigata-shi, Niigata 950-2181, Japan*

[3]*Department of Physics, Tohoku University, Sendai-shi, Miyagi 980-8578, Japan*

[4]*Nagasaki Institute of Applied Science, Nagasaki-shi, Nagasaki 851-0193, Japan*

[5]*Kochi University of Technology, Tosayamada, Kochi 782-8502, Japan*

[6]*Department of Physics, Tokyo University of Science, Noda-shi, Chiba 278-8510, Japan*

[7]*Department of Technical Physics, Peking University, Beijing 100871, People's Republic of China*

[8]*Gesellschaft für Schwerionenforschung (GSI), Planckstrasse 1, D-64291 Darmstadt, Germany*

(Received 1 November 2002; published 31 January 2003)

An attempt was made to find the very neutron-rich isotope ^{21}B among the fragmentation of a 94*A* MeV ^{40}Ar beam. Evidence for the particle instability of ^{21}B was obtained. As part of the search, the production cross sections of 13 light neutron-rich nuclei with Be and Ta targets are presented and compared to previous data. A large enhancement of the production cross sections for a Ta target is shown and a clear energy dependence of the production cross sections is shown for very neutron-rich nuclei.

DOI: 10.1103/PhysRevC.67.014610 PACS number(s): 25.70.Mn, 27.20.+n, 27.30.+t, 21.10.Dr

I. INTRODUCTION

Recently, we surveyed the neutron separation energies and the interaction cross sections for neutron-rich nuclei in the *p-sd* and *sd* shell regions, and found some signature for a new magic number $N=16$ near the neutron drip line [1,2]. If $N=16$ near to the neutron drip line is a good magic number, very neutron-rich ^{21}B may be bound [3]. The nuclear structure of ^{21}B would be interesting, since its A/Z is over 4, which is the largest value among known nuclei. Because of the exceptional A/Z value, an isotope search with a magnetic rigidity setting optimized for this particular nuclide has not yet been performed. Recent developments of radioactive ion (RI) beam technology now turn to allow searches of such nuclei located very far from the stability line (for example, Ref. [4]).

Measurements of the production cross sections (σ_F) are important to assess the feasibility of secondary beam experiments. Recently, very neutron-rich nuclei have received particular interest in view of their exotic structure. It is difficult, however, to predict their σ_F with physical projectile-fragmentation models, such as the abrasion-ablation model [5]. Another approach is to use an empirical parametrization, such as, e.g., the EPAX formula [6]. The quality of such a parametrization depends on reliable experimental data.

^{40}Ar, which is the most neutron-rich stable isotope of Ar, as a beam is widely used for the production of light neutron-rich nuclei due to its easy handling in an ion source and its large abundance (99.6%). Thus, σ_F data for ^{40}Ar would be particularly valuable. Recently, Ozawa *et al.* have measured σ_F from ^{40}Ar fragmentation at relativistic energies ($\sim 1A$ GeV) with a Be target that extends far into the region of neutron-rich isotopes [7]. Also, Momota *et al.* measured σ_F from ^{40}Ar fragmentation at intermediate energies ($\sim 90A$ MeV) with a Be target that covers the region near to stable nuclei [8]. There has been no experiment at intermediate energies to measure σ_F for ^{40}Ar fragmentation that extends far into the region of neutron-rich isotopes. Such measurements are useful to assess the feasibility using a ^{40}Ar beam, especially in a projectile fragment separator for intermediate energies.

One of the interesting features concerning the production of fragments at intermediate energies is that there is a target dependence of σ_F; σ_F for neutron-rich nuclei with a neutron-excess target, for example, Ta, are much larger than those with Be [9]. The fact that there is a target dependence of σ_F at intermediate energies also stimulated us to measure σ_F, although quantitative explanations for the enhancement have not been drawn so far.

In Sec. II of this paper, we describe our experimental setup. In Sec. III, we present an analysis of the data. In Sec. IV, our experimental results are presented and we demonstrate the particle instability of ^{21}B. Our conclusions are given in Sec. V.

II. EXPERIMENTAL SETUP

The experimental setup at RIPS is shown in Fig. 1 [10]. The ^{40}Ar beam accelerated at the AVF and RIKEN Ring Cyclotron up to 94*A* MeV reacted with a 471 mg/cm^2 thick Be target or a 686 mg/cm^2 thick Ta target. The primary beam current was monitored by an array of plastic detectors located near to the production target. The typical primary beam intensity was 40 pnA. The reaction fragments were collected and analyzed by RIPS operated in an achromatic mode with the maximum momentum acceptance (6%) and the solid angle (5 msr).

Particles were identified by a standard method based on the energy loss (ΔE), time-of-flight (TOF), and magnetic

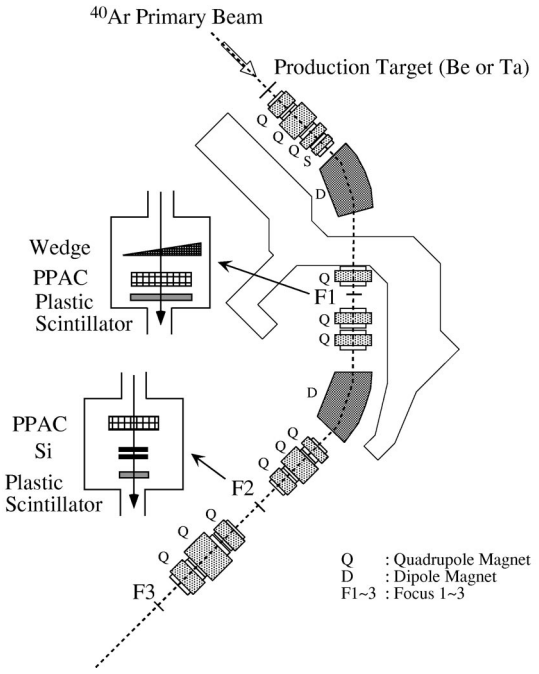

FIG. 1. Experimental setup at the fragment separator RIPS.

TABLE I. List of nuclei for σ_F measurements. The nominal nuclei of the individual settings are underlined. Experimentally determined σ_F for the fragmentation of an ^{40}Ar primary beam in a Be (Ta) target are shown in the second (third) column, respectively.

Nuclei	σ_F (b) on a Be target	σ_F (b) on a Ta target
$\underline{^{25}\mathrm{F}}$	$(4.0\pm1.5)\times10^{-7}$	$(1.05\pm0.31)\times10^{-5}$
$^{23}\mathrm{O}$	$(1.30\pm0.51)\times10^{-7}$	$(3.4\pm1.2)\times10^{-6}$
$\underline{^{24}\mathrm{O}}$	$(5.6\pm2.2)\times10^{-9}$	$(1.17\pm0.33)\times10^{-7}$
$^{26}\mathrm{F}$	$(9.9\pm3.9)\times10^{-9}$	$(2.65\pm0.77)\times10^{-7}$
$^{22}\mathrm{N}$	$(8.9\pm3.5)\times10^{-9}$	$(3.4\pm1.4)\times10^{-7}$
$\underline{^{23}\mathrm{N}}$	$(2.19\pm0.94)\times10^{-10}$	$(3.9\pm2.1)\times10^{-9}$
$^{20}\mathrm{C}$	$(2.17\pm0.50)\times10^{-9}$	$(3.4\pm1.1)\times10^{-8}$
$\underline{^{22}\mathrm{C}}$	$(1.23\pm0.99)\times10^{-12}$	$(7.7\pm4.9)\times10^{-11}$
$\underline{^{19}\mathrm{B}}$	$(3.4\pm1.1)\times10^{-11}$	$(1.59\pm0.48)\times10^{-9}$
$\underline{^{17}\mathrm{B}}$	$(2.91\pm0.45)\times10^{-8}$	$(9.8\pm2.1)\times10^{-7}$
$^{19}\mathrm{C}$	$(1.96\pm0.57)\times10^{-8}$	$(3.16\pm0.69)\times10^{-7}$
$\underline{^{15}\mathrm{B}}$	$(7.0\pm2.7)\times10^{-6}$	$(1.51\pm0.50)\times10^{-4}$
$^{17}\mathrm{C}$	$(5.7\pm2.2)\times10^{-6}$	$(7.3\pm2.1)\times10^{-5}$

rigidity ($B\rho$) measured for each fragment. In this experiment, we identified fragments at $F1$ and $F2$ in RIPS by the $B\rho$-ΔE-TOF method, as follows. The magnetic fields at the two dipoles were monitored by NMR probes. The positions of the fragments at $F1$ were recorded using a parallel-plate avalanche counter (PPAC) to determine the $B\rho$ values. The sensitive area of the PPAC was 15 cm$\times$10 cm, the horizontal size of which covered a full rigidity acceptance of 6% (dispersion at $F1=2.4$ cm/%). The delay-line readout was applied for position reading [11]. The detection efficiencies of the PPAC for B isotopes were more than 90%. A plastic scintillator at $F1$ ($F1$-Pl; thickness$=0.5$ mm) provided timing and analog signals. Thus, the TOF of each fragments was determined from the $F1$-Pl timing to the rf timing, that was provided by the Ring Cyclotron. The flight path from the production target to the $F1$-Pl is 10.4 m. ΔE was provided by the analog signal of $F1$-Pl. Thus, we identified fragments by the $B\rho$-ΔE-TOF method at $F1$.

To reduce the relative rates of light isotopes, such as ^{3}H, a thin aluminum wedge with a mean thickness of 223 mg/cm^2 was used at $F1$. The fragments reached the achromatic focus ($F2$), where a plastic scinitillation counter ($F2$-Pl) with a thickness of 1.5 mm, two silicon detectors (SSDs) with 0.35 mm thickness each, and a PPAC with 10 cm$\times$10 cm effective area were installed. The charge-division read-out was applied to position reading for the PPAC, where the detector efficiency was close to 100% for B isotopes. The TOF of each fragment was determined between the $F2$-Pl timing and the $F1$-Pl timing. The flight path from the $F1$-Pl to the $F2$-Pl is 10.9 m. ΔE was provided by the average of the signals of two SSDs. Thus, we also identified fragments by the $B\rho$-ΔE-TOF method at $F2$.

We used a Ta target for a ^{21}B search. The magnetic rigidity of the first half of RIPS was set at 5.616 Tm in order to optimize the yield of the ^{21}B isotopes. We used the INTENSITY program [12] for the optimization. The magnetic rigidity of the second part of RIPS spectrometer was thereby adjusted to 5.530 Tm. We accumulated data for 150 h.

For σ_F measurements, we used Ta and Be targets. We selected seven nuclei as nominal fragments, as listed in Table I. Thus, we optimized the RIPS setting for these nuclei. We also slightly changed $B\rho$ of RIPS (a few %), several times, for the nominal nuclei to measure σ_F for different $B\rho$ settings. Since RIPS has a large momentum acceptance (6%), RIPS allows us to measure σ_F in the neighborhood of the

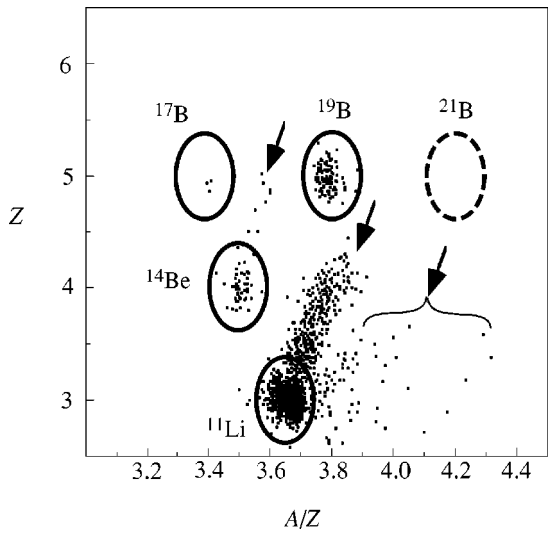

FIG. 2. Two-dimensional plot of Z versus A/Z at $F2$ in RIPS selecting ^{21}B. Visible fragments are shown by circles. The scattered particles are shown by arrows. The position for ^{21}B is shown by a circle with broken lines.

nominal nuclei. Finally, we measured σ_F for 13 nuclei, as listed in Table I.

III. ANALYSIS PROCEDURE

A. Search for ^{21}B

Figure 2 shows a particle-identification spectrum for the ^{21}B search. The charges (Z) and A/Z in the figure were calculated by $B\rho$-ΔE-TOF information at $F2$. As described in Sec. II, we identified particles by the $B\rho$-ΔE-TOF methods at $F1$ and $F2$, independently, in this experiment. In Fig. 2, events that obtained consistent identification at $F1$ are shown in the spectrum. Even by two-step identification at $F1$ and $F2$, scattered events shown by the arrows in Fig. 2 could not be completely cut. However, no scattered events are seen at the position for ^{21}B.

As a conclusion, we did not observe any events for ^{21}B for 150 h of measurements. That allows us to put an upper limit of σ_F for ^{21}B, i.e., 6.7×10^{-14} b, where we assume one event for ^{21}B.

B. Production cross section

In order to determine σ_F, the counting rates of the different isotopes obtained from the two-dimensional spectra, as in Fig. 2, must be corrected for transmission losses in the RIPS for the dead time of the data-acquisition system, and the detection efficiency of PPAC located at $F1$. The dead time was determined in the usual way via two scalers. One scaler recorded all events independent of the data acquisition, whereas the second one counted only those that were registered by the data acquisition. The dead time determined in this way varied by about 5% for different runs. The correction for the detection efficiency at $F1$ PPAC was 3–10 % for B isotopes. For other isotopes (C, N, O, and F), the correction was less than 2%.

The transmission losses were estimated by Monte Carlo–type calculations using the code MOCADI [13]. Here, we also took into account the detector size, the position and the field strength of the magnets. We assumed Gaussian curves for the momentum distributions of the fragments, with widths (σ) according to the Goldhaber formula [14] $\sigma^2=\sigma_0^2A_F(A_P-A_F)/(A_P-1)$, where A_P and A_F refer to the projectile and fragment masses, respectively, and the reduced width $\sigma_0=90$ MeV/c [14]. Thus, we used a calculated momentum distribution for the transmission calculations. According to our simulations, the transmissions from the target to $F2$ were typically 3–10 %.

Finally, the transmission-corrected numbers of counts for the individual isotopes were converted to cross sections using the effective target thicknesses and the number of incident beam particles determined by monitor counters.

The errors of σ_F merit a detailed description. We took into account the following sources of errors: (a) uncertainties of the primary-beam intensity monitor, (b) uncertainties of the transmission calculations, and (c) statistical errors. We calibrated the primary beam monitor twice in the beginning of the experiment. The difference in the two calibrations provides the difference in the primary-beam intensities (~13%).

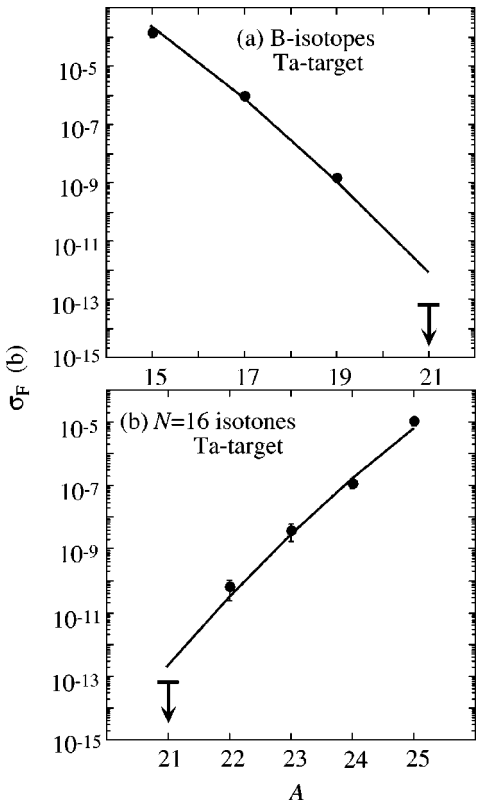

FIG. 3. Experimental production cross sections (σ_F) for B isotopes (a) and $N=16$ isotones (b) with a ^{40}Ar primary beam and 94A MeV in a Ta target. The upper limit of σ_F for ^{21}B is shown by arrows. The solid lines are extrapolations using EPAX2 parametrization [6] normalized to the observed σ_F.

We took into account the value as (a). We measured σ_F several times with different $B\rho$ setting, as described in Sec. II. If the calculated momentum distributions are consistent with the real ones, measured σ_F with different $B\rho$ settings should be consistent each other. However, they were scattered. Thus, we estimated the errors of transmissions calculations based on the deviation from the average (typically ~30%). The statistical errors were estimated based on the number of observed events.

IV. EXPERIMENTAL RESULTS

A. Result of search of ^{21}B

As shown in Fig. 2, we did not observe any events for ^{21}B, and provided the upper limit of σ_F. In Fig. 3, we shows the σ_F for B isotopes (a) and σ_F for $N=16$ isotones (b) with a Ta target. We extrapolated σ_F for ^{21}B using EPAX2 parametrization [6] normalized to the observed σ_F. Thus, we can see that the upper limit of σ_F for ^{21}B is smaller than that by a factor of 12 in (a) and a factor of 3 in (b). This means that we should observe 3 to 12 events of ^{21}B during our measurements if ^{21}B is bound. Thus, data suggest a particle instability of ^{21}B. Among the available mass formula, an infinite nuclear matter model predicted the particle stability of ^{21}B [15]. Improvements in the parametrization for the model are anticipated.

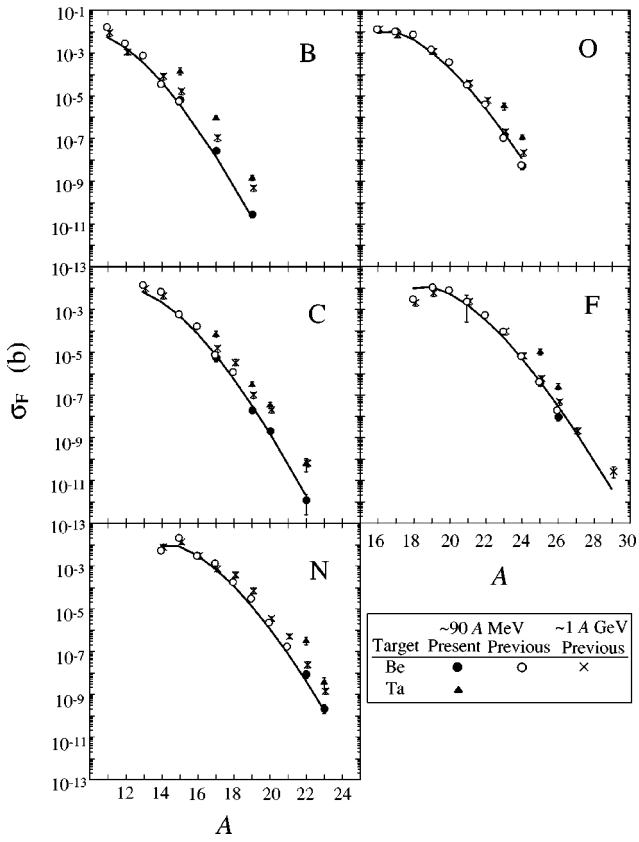

FIG. 4. Experimental production cross sections (σ_F) for B to F isotopes produced with a ^{40}Ar primary beam with Be and Ta targets. The closed circles (triangles) indicate the present data with Be (Ta) targets, respectively. The open circles (cross) indicate the experimental data measured previously with Be targets at 90*A* MeV [8] ($\sim$1*A* GeV [7]), respectively. The σ_F are compared to the EPAX2 formula for a Be target [6] (solid lines).

B. Production cross sections

In Fig. 4, the present experimental results are compared with those measured previously at GSI at $\sim$1*A* GeV [7] and at RIPS at $\sim$90*A* MeV [8] with a Be target. For ^{15}B, ^{17}C, ^{23,24}O, and ^{25,26}F, the present data are very consistent with those measured by Momota *et al.* [8].

In Fig. 4, we see good consistency for σ_F in the data with relativistic energy and those with an intermediate one near to the stable nuclei. However, in neutron-rich nuclei, we can see a clear difference between them. The data with relativistic energy are much larger than those with intermediate energies, for example, a factor 10 difference in ^{19}B, ^{22}C, and ^{23}N. Because σ_F for intermediate energy follows the EPAX2 prediction, the discrepancy suggests an anomalous enhancement of σ_F at relativistic energy. Up to now, the energy dependence of σ_F has not been well studied; for example, even for EPAX2, the energy dependence is not taken into account. Experimental and theoretical studies for the energy dependence of σ_F are anticipated.

In Fig. 5 we show the difference in σ_F between Be and Ta targets. Always, σ_F with a Ta target are larger than those with a Be target by a factor of 10 or more. The enhancement is slightly increased when the nuclei become closer to the drip line. The enhancement is much larger than those calculated by EPAX2, where the difference comes from only the difference in the nuclear size of target. Thus, the different reaction mechanism from projectile fragmentation may be dominant in producing very neutron-rich nuclei in a Ta target. A multistep process for nucleon removal or transfer may be dominant in the production of neutron-rich nuclei in a Ta target at the intermediate energy, since Ta has a much larger number of nucleons compared to Be.

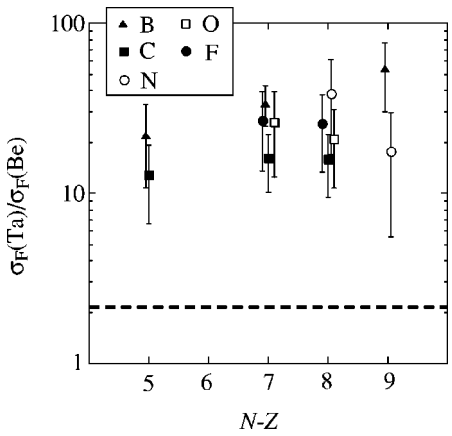

FIG. 5. Neutron number excess ($N-Z$) dependence of the ratio of σ_F with Be and Ta targets [σ_F(Ta)/σ_F(Be)]. The closed triangles, closed squares, open circles, open squares, and closed circles show the data for B, C, N, O, and F isotopes, respectively. The broken line shows the predicted ratio by EPAX2 [6].

V. CONCLUSION

In our experiment, we searched ^{21}B as fragments produced by ^{40}Ar fragmentation in a Ta target at an incident energy of $\sim$94*A* MeV. We searched ^{21}B for 150 h, however, observed no event for the nucleus. As part of the search, we measured the production cross sections for fragments near to the neutron drip line produced by ^{40}Ar fragmentation in Be and Ta targets at an incident energy of $\sim$94*A* MeV. Extrapolated σ_F by the observed σ_F for other B isotopes and other $N=16$ isotones are much larger than the observed upper limit of σ_F of ^{21}B. Thus, the data strongly suggest a particle instability of ^{21}B.

We compared our σ_F data with those measured previously at intermediate energies; good agreement was observed. We also compared our σ_F data with those measured previously at relativistic energies. We found large difference near to the neutron drip line, that suggests the energy dependence of σ_F. We also compared σ_F with Be and Ta targets. A large enhancement of σ_F with a Ta target was confirmed quantitatively.

ACKNOWLEDGMENTS

The authors gratefully acknowledge all of the staff at the RIKEN Ring Cyclotron for insuring smooth operation of the accelerator.

[1] A. Ozawa *et al.*, Phys. Rev. Lett. **84**, 5493 (2000).
[2] R. Kanungo *et al.*, Phys. Lett. B **528**, 58 (2002).
[3] M. Beiner *et al.*, Nucl. Phys. **A249**, 1 (1975).
[4] H. Sakurai *et al.*, Phys. Lett. B **448**, 180 (1999).
[5] J.-J. Gaimard and K.-H. Schmidt, Nucl. Phys. **A531**, 709 (1991).
[6] K. Suemmerer and B. Blank, Phys. Rev. C **61**, 034607 (2000).
[7] A. Ozawa *et al.*, Nucl. Phys. **A673**, 411 (2000).
[8] S. Momota *et al.*, Nucl. Phys. **A701**, 150c (2002).
[9] H. Sakurai *et al.*, Phys. Rev. C **54**, R2802 (1996).
[10] T. Kubo *et al.*, Nucl. Instrum. Methods Phys. Res. B **70**, 309 (1992).
[11] H. Kumagai *et al.*, Nucl. Instrum. Methods Phys. Res. A **470**, 562 (2001).
[12] J. A. Winger *et al.*, Nucl. Instrum. Methods Phys. Res. B **70**, 380 (1992).
[13] N. Iwasa *et al.*, Nucl. Instrum. Methods Phys. Res. B **126**, 284 (1997).
[14] A. S. Goldhaber, Phys. Lett. **53B**, 306 (1974).
[15] R. C. Nayak and L. Satpathy, At. Data Nucl. Data Tables **73**, 213 (1999).